Signal Processing 93 (2013) 3400–3409

Contents lists available at ScienceDirect

Signal Processing

journal homepage: www.elsevier.com/locate/sigpro

Fast maximum likelihood DOA estimation in the two-target case with applications to automotive radar

Philipp Heidenreich [a,*], Abdelhak M. Zoubir [b]

[a] ADC Automotive Distance Control Systems GmbH, Peter-Dornier-Str. 10, 88131 Lindau, Germany
[b] Signal Processing Group, Technische Universität Darmstadt, Merckstr. 25, 64283 Darmstadt, Germany

ARTICLE INFO

Article history:
Received 17 August 2012
Received in revised form
28 February 2013
Accepted 4 March 2013
Available online 21 March 2013

Keywords:
Advanced driver assistance systems
Automotive radar
Direction-of-arrival (DOA)
Maximum likelihood estimation

ABSTRACT

Direction-of-arrival (DOA) estimation of two targets using a single snapshot plays an important role in automotive radar for advanced driver assistance systems. Conventional Fourier methods have a limited resolution and generally yield biased estimates. Subspace methods involve a numerically complex eigendecomposition and require multiple snapshots or a suboptimal pre-processing for reliable estimation. We therefore consider the maximum likelihood (ML) DOA estimator, which is applicable with a single snapshot and shows good statistical properties. To reduce the computational burden, we propose a grid search procedure with a simplified calculation of the objective function. The required projection operators are pre-calculated off-line and stored. To save storage space and computations, we further propose a rotational shift of the field-of-view such that the relevant angular sector, which has to be evaluated, is delimited and centered with respect to broadside. The final estimates are obtained using a quadratic interpolation. The developed method is demonstrated with an example. Simulations are designed to assess the performance of the considered ML estimator with grid search and interpolation, and to compare it among selected representative methods. We further present results obtained with experimental data from a typical application in automotive radar.

1. Introduction

An increasing amount of advanced signal processing algorithms is used in various automotive applications [1–3], e.g., advanced driver assistance systems use various sensors to determine the environment of a vehicle. From an identified traffic situation, these systems regulate the behavior of the vehicle, and instruct or warn the driver in dangerous situations. Often radar sensors are employed, which work reliably even in bad weather conditions, and can provide accurate measurements of the range and relative velocity of multiple targets. A popular modulation scheme in automotive radar is the chirp sequence modulation, [3,4] or [5, Chapter 7]. After the radar pre-processing, consisting of a stretch pulse compression [6, Chapter 8] and a Fourier transform over the pulses, the received data is divided into processing cells, according to range and relative velocity [6,7]. To additionally measure the lateral position of a target, by means of its direction-of-arrival (DOA), an array of antennas in horizontal direction is used. In this case, each processing cell is represented by an array output vector. An automotive radar system of this type is described in [8]. For typical applications such as collision avoidance or adaptive cruise control (ACC), it is essential to accurately estimate the lateral position, and to be able to resolve multiple closely spaced targets. For arrays with limited aperture, this can be achieved with high-resolution processing, which is considered computationally intensive and numerically complex, so that real-time implementation becomes a challenging task.

In most practical situations of automotive radar, multiple targets can be distinguished by their range and/or relative velocity, so that each processing cell contains at most one target. For a single target, the optimal DOA estimates can be

* Corresponding author. Tel.: +49 6151 164595.
E-mail addresses: philipp.heidenreich@continental-corporation.com (P. Heidenreich), zoubir@spg.tu-darmstadt.de (A.M. Zoubir).

0165-1684/$ - see front matter © 2013 Elsevier B.V. All rights reserved.
http://dx.doi.org/10.1016/j.sigpro.2013.03.009

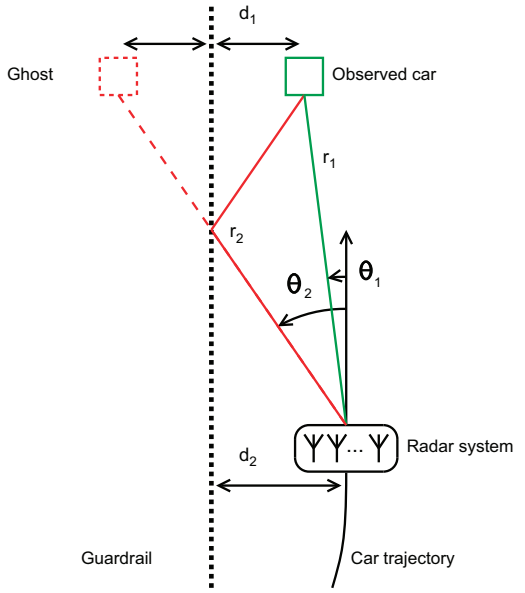

Fig. 1. Automotive radar situation when there is horizontal multipath with a close guardrail. (For interpretation of the references to color in this figure caption, the reader is referred to the web version of this article.)

found using the beamformer (BF) spectrum, which is computationally simple [9]. However, in some situations, multiple target reflections are superposed in a processing cell. In the ACC application, this is motivated by experimental data and may occur when there is horizontal multipath with a close guardrail, as depicted in Fig. 1. If the two propagation paths are not resolved in the BF spectrum, this generally results in a false localization of the observed car, which seems to be pulled towards the guardrail. To identify the multipath situation, and correctly localize the observed car and a ghost target, high-resolution DOA estimation is required. Note that the described problem with two target reflections is very similar to the well-known low angle radar tracking problem [10,11]. Another practically relevant situation with multiple targets per processing cells may occur with slowly moving objects, such as pedestrians, which cannot be distinguished from stationary objects. Here, high-resolution DOA estimation can enhance the pedestrian detection in the neighborhood of a parked car [12].

A number of high-resolution DOA estimators is available in the literature [9,13,14]. Among the subspace methods, there is the popular MUSIC algorithm [15], which requires an eigendecomposition of the spatial covariance matrix, and a one-dimensional search on a fine grid to obtain the DOA estimates. For particular array geometries, there are also analytic solutions, e.g., unitary ESPRIT [16]. Implementing an eigendecomposition on a practical system with real-time constraints can be numerically complex. Eigendecomposition is iterative in nature, and therefore hard to parallelize [17]. Moreover, when only a single snapshot is available, decorrelation techniques are required so that the signal subspace is fully represented. This can be achieved using forward/backward (FB) averaging and spatial smoothing [18], which is suboptimal in general and reduces the array aperture. The described drawbacks can limit the practical usage of subspace methods.

In contrast, the maximum likelihood (ML) DOA estimator of multiple targets can be directly applied with a single snapshot, and can fully benefit from multiple snapshots. It is asymptotically efficient [19], possesses an improved threshold performance when compared to subspace methods [20], and allows to distinguish correlated targets [13]. Despite its good properties, the ML estimator has not enjoyed much practical application due to its high computational cost. It requires the optimization of a multi-dimensional objective function with a complicated multimodal shape. Some existing efficient implementations of ML without eigendecomposition are the IQML method [21], the RELAX algorithm [22], or the method of alternating projections [23]. All mentioned methods are iterative, which can limit the applicability on practical systems with real-time constraints. For two closely spaced targets, there is also a computationally attractive non-iterative ML variant in beamspace [11].

Unlike array processing with multiple snapshots, the case with a single snapshot has not received much attention in the literature. In the context of automotive radar, it is also studied in [24]. In [25], an approach is proposed for two closely spaced targets, based on the knowledge of the DOA centroid an a first-order approximation of the MUSIC projector. A Bayesian framework is considered in [26]. An ESPRIT method with a synthetically increased aperture is presented in [27].

In this paper, we consider the situation with one or two targets in a processing cell as practically relevant. For DOA estimation and detection, an optimal approach, based on ML estimation and a generalized likelihood ratio test (GLRT) is applied. For ML estimation in the two-target case, we consider a global search over a selected two-dimensional grid as a suitable implementation. An interpolation in the neighborhood of the optimum is used to obtain the final estimate [14]. To reduce the computational burden, we propose a simplified calculation of the objective function. The required projection operators are data-independent and can be pre-calculated off-line, which enables a trade-off between computational complexity and storage space. To save storage space and computations, we further propose a rotational shift of the field-of-view such that the relevant angular sector, which has to be evaluated, is delimited and centered with respect to broadside. The proposed technique is non-iterative and well suited for a fast implementation on a practical system, since the calculation of the objective function is only based on independent multiply–add operations, which is easy to parallelize.

We note that the results obtained with experimental data presented here have also been reported in [28]. This paper offers a more detailed treatment, in particular, a simulative performance assessment and comparison among selected representative methods.

2. Preliminaries

2.1. Signal model

The received radar signals from target reflections can be distinguished by the time delay and the Doppler shift,

according to range and relative velocity of the target, respectively. Using radar pre-processing, we can extract specific processing cells, corresponding to range and relative velocity [7]. Each processing cell represents a single array output vector, or snapshot, modeled by

$$\boldsymbol{x} = \boldsymbol{x}_D(\boldsymbol{\eta}_D) + \boldsymbol{n} \tag{1}$$

where

$$\boldsymbol{x}_D(\boldsymbol{\eta}_D) = \sum_{k=1}^{D} s_k \boldsymbol{a}(\phi_k) \tag{2}$$

is the signal component and $\boldsymbol{n}$ is a noise vector. D is the number of targets superposed in a processing cell, s_k and ϕ_k denote the complex-valued target response parameter and DOA parameter in electrical angle, respectively. The unknown signal parameters are collected in $\boldsymbol{\eta}_D = [s_1,\ldots,\ s_D,\phi_1,\ldots,\phi_D]^T$.

Noise vector $\boldsymbol{n}$ is assumed to be spatially white, circular complex Gaussian distributed with zero mean and common variance σ^2.

Without loss of generality, the steering vector of the M-element uniform linear array (ULA) can be defined as

$$\boldsymbol{a}(\phi) = e^{-j(M-1)\phi/2}[1, e^{j\phi},\ldots,e^{j(M-1)\phi}]^T \tag{3}$$

so that the phase center is located at the origin of the coordinate system. The spatial angle θ is directly related to the electrical angle $\phi = \kappa d \sin(\theta)$, where $\kappa = 2\pi/\lambda$, λ is the wavelength, and d is the sensor spacing.

We assume a calibrated array, i.e., the remaining imperfections after calibration [14] are negligible when compared to the measurement noise. To preserve the ULA steering vector structure, a calibrated snapshot is obtained as $\boldsymbol{x} = \boldsymbol{Q}^{-1}\tilde{\boldsymbol{x}}$, where $\boldsymbol{Q}$ is a direction-independent correction matrix, obtained from off-line measurements, and $\tilde{\boldsymbol{x}}$ is an uncalibrated snapshot. An additional calibration of direction-dependent errors in automotive radar has been considered in [29,30].

2.2. Target detection

In this paper, we focus on ML estimation in the two-target case. However, since the single-target case is predominant in automotive radar, a target detection procedure is considered first. The GLRT for deciding between the single-target and the two-target situation, i.e., (1) with $D=1$ and $D=2$, is [31]

$$\Lambda = \frac{\max_{\boldsymbol{\eta}_2,\sigma^2} p_2(\boldsymbol{x}|\boldsymbol{\eta}_2,\sigma^2)}{\max_{\boldsymbol{\eta}_1,\sigma^2} p_1(\boldsymbol{x}|\boldsymbol{\eta}_1,\sigma^2)} > \gamma$$

where $p_k(\boldsymbol{x}|\boldsymbol{\eta}_k,\sigma^2)$ is the conditional probability density function of the snapshot given unknown parameters, or likelihood function. When test statistic Λ exceeds threshold γ, the single-target situation is rejected and the two-target situation is considered as more likely.

Evaluating Λ involves determining the respective ML estimates. For the above signal model with spatially white Gaussian noise, the GLRT can be simplified to [32]

$$\log\Lambda = M\log\hat{\sigma}_1^2 - M\log\hat{\sigma}_2^2 > \log\gamma \tag{4}$$

where

$$\hat{\sigma}_k^2 = \frac{1}{M}\|\boldsymbol{x}-\boldsymbol{x}_k(\hat{\boldsymbol{\eta}}_k)\|^2$$

and $\hat{\boldsymbol{\eta}}_k$, $k=1,2$ denote the corresponding ML estimates.

2.3. Maximum likelihood estimation

The ML estimates of DOA parameters are obtained by optimizing a D-dimensional objective function $c(\cdot)$ [9,13]

$$\{\hat{\phi}_1,\ldots,\hat{\phi}_D\} = \arg\max_{\phi_1,\ldots,\phi_D} \underbrace{\|\boldsymbol{P}_{\boldsymbol{A}}(\phi_1,\ldots,\phi_D)\boldsymbol{x}\|^2}_{c(\phi_1,\ldots,\phi_D)} \tag{5}$$

where

$$\boldsymbol{P}_{\boldsymbol{A}}(\phi_1,\ldots,\phi_D) = \boldsymbol{A}(\boldsymbol{A}^H\boldsymbol{A})^{-1}\boldsymbol{A}^H \tag{6}$$

is the projection matrix onto the column span of the steering matrix $\boldsymbol{A} = [\boldsymbol{a}(\phi_1),\ldots,\boldsymbol{a}(\phi_D)]$.

An intuitive interpretation is that we seek for DOA parameters $\phi_1,\ldots,\phi_D$ which maximize the projection of $\boldsymbol{x}$ onto the plane spanned by the columns of $\boldsymbol{A}$.

The target response parameters can be obtained by

$$\hat{\boldsymbol{s}} = [\hat{s}_1,\ldots,\hat{s}_D]^T = [\boldsymbol{a}(\hat{\phi}_1),\ldots,\boldsymbol{a}(\hat{\phi}_D)]^{\#}\boldsymbol{x}$$

where $(\cdot)^{\#}$ denotes the Moore–Penrose pseudoinverse operator.

In the single-target case, the objective function in (5) reduces to the well-known BF spectrum

$$c(\phi_1) = \frac{1}{M}|\boldsymbol{a}(\phi_1)^H\boldsymbol{x}|^2$$

which is the spatial equivalent of the periodogram and can be efficiently calculated using an FFT with zero-padding. Due to its simplicity, the BF spectrum is often used for DOA estimation of multiple targets. However, it cannot resolve closely spaced targets, which are spaced by less than the Rayleigh beamwidth $\mathrm{BW} = 2\pi/M$. Even if the targets are resolved, there is a non-negligible estimation bias due to the leakage effect.

In the following, we focus on the two-target case, and describe a direct evaluation of the objective function in (5), a global search strategy and a quadratic interpolation.

2.3.1. Direct objective function evaluation

In the two-target case, the determination of the projection matrix requires the matrix inverse of $\boldsymbol{A}^H\boldsymbol{A}$, which is of dimension two. Using the respective inversion formula, and notation $\boldsymbol{a}_1 = \boldsymbol{a}(\phi_1)$ and $\boldsymbol{a}_2 = \boldsymbol{a}(\phi_2)$ for convenience, we have

$$\boldsymbol{P}_{\boldsymbol{A}}(\phi_1,\phi_2) = \frac{1}{M^2-\beta^2}(M\boldsymbol{a}_1\boldsymbol{a}_1^H - \beta\boldsymbol{a}_1\boldsymbol{a}_2^H - \beta\boldsymbol{a}_2\boldsymbol{a}_1^H + M\boldsymbol{a}_2\boldsymbol{a}_2^H)$$

with real-valued $\beta = \boldsymbol{a}_1^H\boldsymbol{a}_2$, and it has been used that $\boldsymbol{a}_1^H\boldsymbol{a}_1 = M$. This allows to directly calculate

$$c(\phi_1,\phi_2) = \frac{1}{M^2-\beta^2}(M|y_1|^2 - 2\beta\mathrm{Re}\{y_1^*y_2\} + M|y_2|^2) \tag{7}$$

where $y_1 = \boldsymbol{a}_1^H\boldsymbol{x}$ and $y_2 = \boldsymbol{a}_2^H\boldsymbol{x}$.

Provided all steering vectors are available on a discrete grid, a significant part of the computational cost, required for a single point of the objective function in (7), constitutes

the calculation of β, y_1 and y_2, which corresponds to $10M$ real-valued multiply–add operations.

2.3.2. Global search

Due to the complicated multimodal shape of objective function $c(\phi_1,\phi_2)$, a numerical search procedure such as a damped Newton method critically depends on the initialization [33]. A reliable initialization without eigendecomposition appears difficult to find, especially when the targets are not resolved in the BF spectrum. Here, we consider a global evaluation of the two-dimensional objective function on a selected grid. Unlike numerical search procedures, this allows a non-iterative implementation.

Due to the symmetry of the ML objective function, a global evaluation is required for $\phi_1 < \phi_2$ only. The resulting triangular search range is shown in Fig. 2 (left). The corresponding computational cost is

$$C = C_1 N_2, \quad N_2 = \frac{(N_\phi - 1)N_\phi}{2}$$

where C_1 is the computational cost, required to evaluate a single point of the objective function, N_2 is the number of points in the two-dimensional search range, and N_ϕ is the number of grid points in the field-of-view, which is inversely proportional to the grid size $\Delta\phi$.

When the global search is carried out on a discrete grid, the estimation accuracy is limited by $\Delta\phi$. The final estimate can be improved by an interpolation in the neighborhood of the optimum [14], which is described next.

2.3.3. Quadratic interpolation

Let $c(\phi_1,\phi_2)$ be evaluated on a discrete grid with $\Delta\phi$. Let the maximum occur at index m and n and corresponding positions $\phi_{1,m}$ and $\phi_{2,n}$. Further, let a two-dimensional elliptic paraboloid function be given by

$$\tilde{c}(\phi_1,\phi_2) = \alpha_1(\phi_1 - \hat{\phi}_1)^2 + \alpha_2(\phi_2 - \hat{\phi}_2)^2 + \hat{c}$$

where α_1 and α_2 are the paraboloid width parameters, $\hat{\phi}_1$ and $\hat{\phi}_2$ are the desired refined peak positions, and $\hat{c}$ is a refined peak value. We can set up a system of equations by evaluating the paraboloid function at peak index (m,n) and its direct neighbors $(m\pm1,n)$ and $(m,n\pm1)$, where the corresponding values of the cost function are denoted by $c_{m,n}$, $c_{m\pm1,n}$ and $c_{m,n\pm1}$. Solving for the unknown parameters, we obtain

$$\hat{\phi}_1 = \phi_{1,m} + 0.5\Delta\phi \frac{c_{m-1,n} - c_{m+1,n}}{c_{m-1,n} - 2c_{m,n} + c_{m+1,n}}$$

$$\hat{\phi}_2 = \phi_{2,n} + 0.5\Delta\phi \frac{c_{m,n-1} - c_{m,n+1}}{c_{m,n-1} - 2c_{m,n} + c_{m,n+1}}$$

Note that estimates for $\hat{\phi}_1$ and $\hat{\phi}_2$ are decoupled, and correspond to a simple one-dimensional quadratic interpolation.

We remark that the quadratic interpolation approach is used for the sake of simplicity. Also, it is motivated by the commonly applied quadratic approximation of a sinc function, to which the ML objective function decouples for well separated targets. A simulation example is used to demonstrate the interpolation gain of this approach when varying angular separation $\phi_2 - \phi_1$ and grid size $\Delta\phi$.

3. Proposed approach

If multiple snapshots of the same processing cell, say at different cycles n, are considered, model (1) extends to $\boldsymbol{x}[n]$, $n = 1,\ldots,N$, where N is the number of available snapshots. In this case, the ML objective function for $D=2$ targets extends to

$$c(\phi_1,\phi_2) = \frac{1}{N}\sum_{n=1}^{N} \|\boldsymbol{P}_{\boldsymbol{A}}(\phi_1,\phi_2)\boldsymbol{x}[n]\|^2 = \mathrm{Tr}\{\boldsymbol{P}_{\boldsymbol{A}}(\phi_1,\phi_2)\hat{\boldsymbol{R}}\} \tag{8}$$

where

$$\hat{\boldsymbol{R}} = \frac{1}{N}\sum_{n=1}^{N} \boldsymbol{x}[n]\boldsymbol{x}[n]^H$$

is the sample covariance matrix.

We remark that the single-snapshot case is of primary importance for the considered application. However, to enhance DOA estimation accuracy, it may be desirable to combine multiple snapshots, which have been associated in a tracking procedure. Therefore, we also consider the general case with N snapshots and comment on the special case with $N=1$. Note that for $N>1$, one has to trade off between the evaluation of the quadratic term and the trace notation in (8).

In the following we aim at reducing the computational cost of the global search [28]. First, we exploit the structure of the projection matrix to derive a simplified calculation of the objective function, where the required projection operators are pre-calculated off-line and stored. Second, to save storage space and computations, we consider a delimited search range, based on a circular shift of the field-of-view. Finally, we present an example to demonstrate the developed approach.

3.1. Simplified objective function calculation

It is easily shown that projection matrices of ULA steering vectors, such as defined in (3), are centro-Hermitian [28,32], i.e., they remain unchanged after complex conjugation and interchanging the columns and rows,

$$\boldsymbol{J}_M \boldsymbol{P}_{\boldsymbol{A}}(\phi_1,\phi_2)^* \boldsymbol{J}_M = \boldsymbol{P}_{\boldsymbol{A}}(\phi_1,\phi_2)$$

where $\boldsymbol{J}_M$ denotes the exchange matrix of dimension M, with ones on the anti-diagonal and zeros elsewhere.

Using this property, it can be easily shown that the ML objective function remains unchanged when $\boldsymbol{x}$ is replaced by its complex conjugated backward version $\boldsymbol{J}_M\boldsymbol{x}^*$. Hence, (8) remains unchanged when FB averaging is applied, so that we can replace $\hat{\boldsymbol{R}}$ with

$$\hat{\boldsymbol{R}}_{\mathrm{FB}} = \frac{1}{2}(\hat{\boldsymbol{R}} + \boldsymbol{J}_M\hat{\boldsymbol{R}}^*\boldsymbol{J}_M)$$

which is centro-Hermitian by definition.

3.1.1. Unitary transformation

To simplify the calculation (8), we use the centro-Hermitian property of $\boldsymbol{P}_{\boldsymbol{A}}$ and $\hat{\boldsymbol{R}}_{\mathrm{FB}}$, and the idea in [34]. We begin with the trace notation, as it is based on the

sample covariance matrix and can be directly applied in the multiple-snapshot case.

Let $\boldsymbol{Q}_M$ be a unitary column conjugate symmetric matrix, which satisfies $\boldsymbol{J}_M\boldsymbol{Q}_M^*=\boldsymbol{Q}_M$. A sparse choice is

$$\boldsymbol{Q}_{2m+1}=\frac{1}{\sqrt{2}}\begin{bmatrix}\boldsymbol{I}_m & \boldsymbol{0} & j\boldsymbol{I}_m\\ \boldsymbol{0}^T & \sqrt{2} & \boldsymbol{0}^T\\ \boldsymbol{J}_m & \boldsymbol{0} & -j\boldsymbol{J}_m\end{bmatrix}$$

where $M=2m+1$ and $\boldsymbol{I}_m$ denotes the identity matrix of dimension m. An equivalent unitary matrix of dimension $2m$ is obtained by deleting the center row and center column of $\boldsymbol{Q}_{2m+1}$.

The main result of [34] is that any square centro-Hermitian matrix is equivalently expressed by a real-valued matrix of the same dimension by means of a unitary transformation. The real-valued quantities for the sample covariance matrix and projection matrix, respectively, are obtained by

$$\hat{\boldsymbol{C}}=\boldsymbol{Q}_M^H\hat{\boldsymbol{R}}_{\mathrm{FB}}\boldsymbol{Q}_M \tag{9}$$

$$\boldsymbol{V}(\phi_1,\phi_2)=\boldsymbol{Q}_M^H\boldsymbol{P}_{\boldsymbol{A}}(\phi_1,\phi_2)\boldsymbol{Q}_M. \tag{10}$$

A similar approach has been used in [16,35] to derive the unitary ESPRIT and unitary root-MUSIC algorithm, respectively, in which computational cost is reduced by replacing a complex-valued by a real-valued eigendecomposition.

Since we have $\boldsymbol{Q}_M\boldsymbol{Q}_M^H=\boldsymbol{I}_M$, the objective function in (8) can be rewritten as

$$\begin{aligned}c(\phi_1,\phi_2)&=\mathrm{Tr}\{\boldsymbol{P}_{\boldsymbol{A}}(\phi_1,\phi_2)\hat{\boldsymbol{R}}\}\\&=\mathrm{Tr}\{\boldsymbol{P}_{\boldsymbol{A}}(\phi_1,\phi_2)\boldsymbol{Q}_M\boldsymbol{Q}_M^H\hat{\boldsymbol{R}}_{\mathrm{FB}}\boldsymbol{Q}_M\boldsymbol{Q}_M^H\}\\&=\mathrm{Tr}\{\boldsymbol{Q}_M^H\boldsymbol{P}_{\boldsymbol{A}}(\phi_1,\phi_2)\boldsymbol{Q}_M\boldsymbol{Q}_M^H\hat{\boldsymbol{R}}_{\mathrm{FB}}\boldsymbol{Q}_M\}\\&=\mathrm{Tr}\{\boldsymbol{V}(\phi_1,\phi_2)\hat{\boldsymbol{C}}\}.\end{aligned} \tag{11}$$

To simplify the computation of the trace in (11), only the diagonal entries of the matrix product are required. Also, we exploit that real-valued matrices $\boldsymbol{V}(\phi_1,\phi_2)$ and $\hat{\boldsymbol{C}}$ are symmetric, so that the computation of the trace in (11) can further be reduced. Towards this end, let

$$\mathrm{sym}\{\boldsymbol{F}\}=[f_{11},f_{12},f_{22},f_{13},f_{23},f_{33},f_{14},\ldots,f_{MM}]^T$$

which selects matrix elements f_{mn}, $m\le n$ from symmetric $\boldsymbol{F}\in\mathbb{R}^{M\times M}$ and stacks them into a vector of dimension $M(M+1)/2$. Thereby, redundant matrix entries are removed. Further, let $\boldsymbol{l}=[1,2,1,2,2,1,2,\ldots,1]^T$ be a scaling vector of the same dimension, being two for off-diagonal entries and one for diagonal entries of sym$\{\boldsymbol{F}\}$. Now, we can rewrite

$$c(\phi_1,\phi_2)=\mathrm{Tr}\{\boldsymbol{V}(\phi_1,\phi_2)\hat{\boldsymbol{C}}\}=\boldsymbol{v}(\phi_1,\phi_2)^T\hat{\boldsymbol{c}} \tag{12}$$

with

$$\begin{aligned}\boldsymbol{v}(\phi_1,\phi_2)&=\mathrm{sym}\{\boldsymbol{V}(\phi_1,\phi_2)^T\}\odot\boldsymbol{l}\\\hat{\boldsymbol{c}}&=\mathrm{sym}\{\hat{\boldsymbol{C}}\}\end{aligned}$$

where $\odot$ denotes the element-wise Hadamard product.

Clearly, the projection operator $\boldsymbol{v}(\phi_1,\phi_2)$ is data-independent. The key idea for a fast implementation is that $\boldsymbol{v}(\phi_1,\phi_2)$ is pre-calculated off-line for every point $\phi_1<\phi_2$ in the search range, and stored. In this case, the simplified calculation using (12) only requires $C_1=M(M+1)/2$ real-valued multiply–add operations. Note that $\hat{\boldsymbol{c}}$ has to be calculated only once. The required storage space for the projection operators is $N_2M(M+1)/2$ real-valued numbers.

3.1.2. Single-snapshot alternative

In the single-snapshot case, an alternative is to employ an eigendecomposition of (10),

$$\boldsymbol{V}(\phi_1,\phi_2)=\boldsymbol{v}_1\boldsymbol{v}_1^T+\boldsymbol{v}_2\boldsymbol{v}_2^T$$

with eigenvectors $\boldsymbol{v}_1,\boldsymbol{v}_2\in\mathbb{R}^{M\times 1}$. For convenience, the dependence on ϕ_1 and ϕ_2 is omitted. Using $\boldsymbol{y}=\boldsymbol{Q}_M^H\boldsymbol{x}$, the objective function can be rewritten as

$$c(\phi_1,\phi_2)=\boldsymbol{y}^H(\boldsymbol{v}_1\boldsymbol{v}_1^T+\boldsymbol{v}_2\boldsymbol{v}_2^T)\boldsymbol{y}=|z_1|^2+|z_2|^2 \tag{13}$$

where $z_1=\boldsymbol{v}_1^T\boldsymbol{y}$ and $z_2=\boldsymbol{v}_2^T\boldsymbol{y}$.

Likewise, to achieve a fast implementation, the projection operator eigenvectors, $\boldsymbol{v}_1$ and $\boldsymbol{v}_2$, are pre-calculated off-line for every point $\phi_1<\phi_2$ in the search range, and stored. In this case, a significant part of (13) constitutes the calculation of z_1 and z_2, which corresponds to $4M$ real-valued multiply–add operations. The required storage space for the projection operator eigenvectors is $N_2 2M$ real-valued numbers.

3.1.3. Comparison

The overall cost of a global search has been described in Section 2.3.2. The calculation of projection operators is done off-line and does not contribute to the overall cost. Also, the pre-processing, such as the formation of the covariance matrix, has no significant effect, as it is performed only once. For the single-snapshot case, a trade-off between C_1 (real-valued multiply–add operations) and the required storage space (real-valued numbers) is given in Table 1.

In the single-snapshot case, and considering $M=8$, the simplified objective function in (13) slightly outperforms (12), both in terms of required computations and storage space. However, when multiple snapshots are available, the simplified objective function in (12) is preferred. The presented methods allow a trade-off between computational cost and storage space, which is achieved by a pre-calculation of data-independent projection operators.

We have seen in Table 1 that the storage space grows with N_ϕ. Also, the DOA estimation performance in terms of accuracy and resolution is directly influenced by the grid size $\Delta\phi$, and thus by N_ϕ. Since the storage space may be limited on a practical system, we propose to save storage space and computations in the next section.

3.2. Delimited search range

We consider the more difficult case of closely spaced targets, which are unresolved in the BF spectrum, i.e., $\phi_2-\phi_1<\mathrm{BW}$. Note that when the targets are well separated and resolved in the BF spectrum, high-resolution DOA estimation is not necessary. In this case, a computationally simple strategy for reducing the DOA estimation bias is possible [36].

Let $\hat{\phi}_0\in[\phi_1,\phi_2]$ be an estimate of the midpoint of the unresolved targets, e.g. obtained from the BF spectrum.

Table 1
Computations required for calculating the objective function and storage space, in the single-snapshot case.

	C_1	Storage space
Direct (7)	$\approx 10M$	$N_\phi 2M$
Simplified (12)	$M(M+1)/2$	$N_2 M(M+1)/2$
Simplified (13)	$\approx 4M$	$N_2 2M$

Consider the shifted array output model, which corresponds to a rotational shift of the field-of-view

$$\boldsymbol{x}' = \boldsymbol{x} \odot \boldsymbol{a}(\hat{\phi}_0)^* = s_1 \boldsymbol{a}(\phi_1') + s_2 \boldsymbol{a}(\phi_2') + \boldsymbol{n}' \tag{14}$$

where $\phi_1' = \phi_1 - \hat{\phi}_0$ and $\phi_2' = \phi_2 - \hat{\phi}_0$ are the shifted DOA parameters, centered with respect to broadside. The random characteristics of the shifted noise vector $\boldsymbol{n}' = \boldsymbol{n} \odot \boldsymbol{a}(\hat{\phi}_0)^*$ remain unchanged.

This rotational shift allows to evaluate $c(\phi_1', \phi_2')$ only on a delimited search range, e.g., $\phi' \in [-1.5\mathrm{BW}, 1.5\mathrm{BW}]$, which very likely contains the centered DOA parameters ϕ_1' and ϕ_2'. As a result, the number of points in the search range, N_2, and therewith the storage space of the projection operators, has been reduced significantly.

3.3. Example

An example is presented to demonstrate the delimited search range. We consider a ULA with $M=8$ elements, spaced by $\lambda/2$. A noise-free snapshot with two targets is simulated according to (2). We use $s_1 = 1$, $s_2 = 1/\sqrt{2} e^{j\pi/3}$, and $\phi_2 - \phi_1 = \mathrm{BW}/2$.

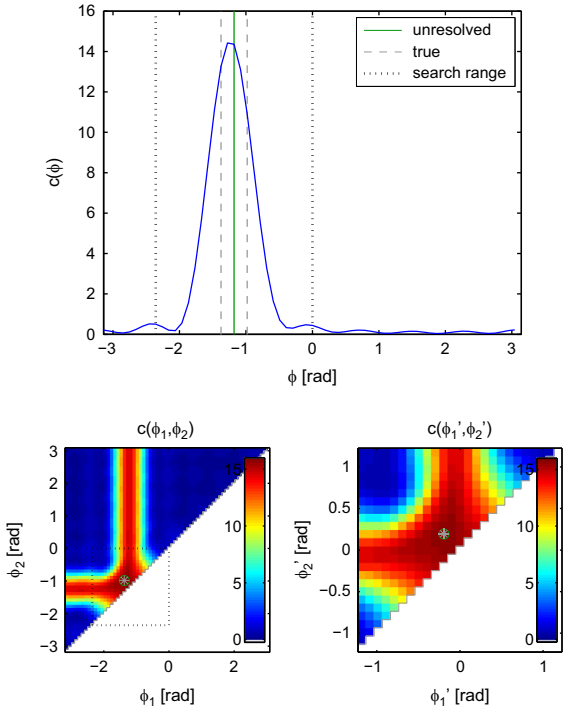

Fig. 2. Example, ULA with $M=8$, noise-free snapshot with two targets separated by $\phi_2 - \phi_1 = \mathrm{BW}/2$: BF spectrum to identify relevant angular sector (top), ML objective function with grid size $\Delta\phi = 2\pi/64$, for full search range (left), and shifted and delimited search range (right).

The targets are unresolved in the corresponding BF spectrum, as shown in Fig. 2 (top). The unresolved peak position can be used for identifying the relevant angular sector for the delimited search range. Fig. 2 also shows the ML objective function with grid size $\Delta\phi = 2\pi/64$, for the full search range (left), and for the shifted and delimited search range (right).

In this example, N_2 has been reduced from 2016 to 276.

4. Performance assessment

Simulations are used to assess the performance of the considered ML estimator with grid search and interpolation, and to compare it with the Cramér–Rao bound (CRB) and among selected representative methods.

We expect the ML estimator as a benchmark algorithm, especially regarding its threshold performance for closely spaced targets and at moderate SNR [20]. The limits for the estimation accuracy are expected due to the finite grid and the quadratic interpolation. Thus, we present a simulation example to study the interpolation gain. Furthermore, we compare the considered ML estimator among selected representative methods: two iterative ML implementations, the two-target analytic ML algorithm in beamspace [11] and unitary ESPRIT.

4.1. Simulation setup

As in the example, we consider a ULA with $M=8$ elements, spaced by $\lambda/2$. Single snapshots with two targets are simulated according to (1). We use $s_1 = 1$ and $s_2 = (\frac{1}{2})^{1/2} e^{j\varphi}$, where φ is uniformly distributed between 0 and 2π. The SNR is defined with respect to the stronger target. For a fair assessment of the grid search DOA estimation, in each simulation run, we add a random jitter to ϕ_1 and ϕ_2, which is uniformly distributed between $\pm \Delta\phi/2$.

We use the spatial angle θ for calculating estimation errors. As a performance metric, the averaged root mean square error is defined as

$$\mathrm{RMSE}^2 = \frac{1}{2}\left[\frac{1}{\mathrm{MC}} \sum_{m=1}^{\mathrm{MC}} (\hat{\theta}_{1,m} - \theta_1)^2 + (\hat{\theta}_{2,m} - \theta_2)^2\right]$$

where $\hat{\theta}_{1,m}$ and $\hat{\theta}_{2,m}$ are the DOA estimates in run m, and MC is the number of Monte-Carlo runs. We use $\mathrm{MC} = 10^4$.

To give an indication of the resolution performance of the presented algorithms, we only display simulation points for which 95% of runs are successfully resolved, i.e., the DOA estimates are sufficiently close to the true parameters, and the following condition is fulfilled

$$|\hat{\theta}_{1,m} - \theta_1| < \tfrac{1}{2}(\theta_2 - \theta_1) \cap |\hat{\theta}_{2,m} - \theta_2| < \frac{1}{2}(\theta_2 - \theta_1).$$

4.2. Cramér–Rao bound

The CRB for estimating parameters ϕ_1 and ϕ_2 from snapshot $\boldsymbol{x}$ in (1) with $D=2$ is given by [19]

$$\mathbf{CRB}_\phi = \frac{\sigma^2}{2} \mathrm{Re}\{(\boldsymbol{D}^H[\boldsymbol{I} - \boldsymbol{P}_{\boldsymbol{A}}]\boldsymbol{D}) \odot (\boldsymbol{s}\boldsymbol{s}^H)^T\}^{-1}$$

where

$$\boldsymbol{D} = [\boldsymbol{d}(\phi_1), \boldsymbol{d}(\phi_2)], \quad \boldsymbol{d}(\phi) = \frac{\partial \boldsymbol{a}(\phi)}{\partial \phi}$$

is a matrix of differential steering vectors and projection matrix $\boldsymbol{P}_{\boldsymbol{A}}$ is defined in Section 2.3. The diagonal elements of $\mathbf{CRB}_{\phi}$ represent a lower bound on the average estimation error variance. When spatial angles are used instead of electrical angles, the CRB is modified to

$$\mathbf{CRB}_{\theta} = \boldsymbol{G}^{-1}\mathbf{CRB}_{\phi}\boldsymbol{G}^{-1}$$

where $\boldsymbol{G} = \mathrm{diag}\{\kappa d \cos(\theta_1), \kappa d \cos(\theta_2)\}$.

4.3. Interpolation gain

To study the interpolation gain, we consider a relatively high SNR of 40 dB. We simulate the performance of the proposed method, calculated via (12), with grid sizes $\Delta\phi = 2\pi/64$, $2\pi/128$, and $2\pi/256$. Fig. 3 shows the averaged RMSE as a function of angular separation $\theta_2 - \theta_1$, for various grid sizes, with interpolation (solid lines) and without interpolation (dashed lines).

One can observe that without interpolation, the estimation accuracy saturates at the indicated analytical quantization error, corresponding to the standard deviation of a uniform distribution between $\pm\Delta\phi/2$. Despite the simple quadratic interpolation approach, the interpolation gain can be significant, and generally depends on the angular separation. Note, however, that a performance close to the CRB can only be achieved with very small grid sizes.

Often in practice, a certain estimation accuracy is sufficient to realize some functionality. In the following, we consider grid size $\Delta\phi = 2\pi/128$, which allows a good compromise between estimation accuracy and computational cost.

4.4. Comparison among representative methods

We compare the developed ML estimator with grid search and interpolation among selected representative methods. First, two iterative ML implementations without eigendecomposition are considered:

- The method of alternating projections (AP) [23] optimizes the ML objective function in (5) by transforming it into an iterative sequence of one-dimensional optimization problems. In each iteration an optimization is performed with respect to a single parameter while the remaining parameters are held fixed. This includes the projection of the array response onto the nullspace of the steering matrix of the remaining parameters. For a comparable grid search, we use the same $\Delta\phi$ and a one-dimensional quadratic interpolation.
- The iterative quadratic maximum likelihood (IQML) algorithm [21] reparameterizes the projection matrix with a linear prediction polynomial, whose order corresponds to the number of targets. In each iteration, a symmetric banded Toeplitz matrix has to be inverted, and the new polynomial coefficients result from solving the normal equations of a whitened covariance matrix. After convergence, the DOA estimates are obtained by polynomial rooting.

Second, we consider two other computationally efficient algorithms:

- The two-target ML algorithm in beamspace [11] is a computationally appealing technique, and has been developed in the context of low angle radar tracking. The beamspace array output vectors are formed using three orthogonal beams. In this case, for $N \geq 3$, the DOA estimates can be obtained analytically by solving a second order polynomial, whose coefficients result from solving the normal equations of a beamspace covariance matrix. In the single-snapshot case, we synthetically generate multiple snapshots by using three overlapping subarrays [18].
- Unitary ESPRIT is a subspace method with reduced computational cost [16]. It only requires the eigendecomposition of the real-valued spatial covariance matrix $\hat{\boldsymbol{C}}$, as in (9). The DOA estimates are obtained analytically, by solving a least-squares problem and an eigendecomposition of dimension two, for two targets. In the single-snapshot case, we also synthetically generate three snapshots by using overlapping subarrays.

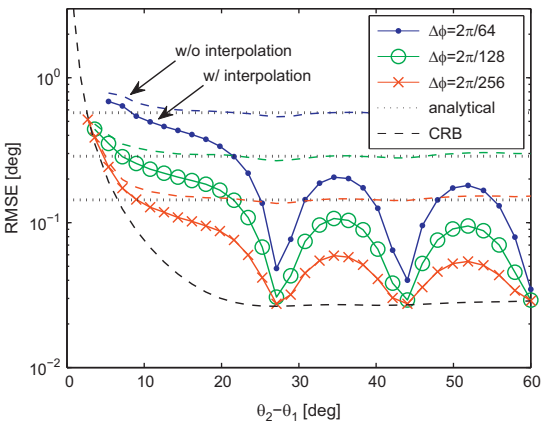

Fig. 3. Performance comparison with interpolation and without, for various step sizes $\Delta\phi$, averaged RMSE versus angular separation $\theta_2 - \theta_1$, with SNR = 40 dB and $N = 1$.

For the comparison among the described two iterative ML implementations and two other computationally efficient algorithms, Fig. 4 shows the averaged RMSE as a function of SNR for $\phi_2 - \phi_1 = \mathrm{BW}/2$, which corresponds to $\theta_2 - \theta_1 \approx 7.2^{\circ}$.

One can observe that the ML estimator with grid search and interpolation shows a good threshold performance for small SNR, and converges to finite accuracy due to the chosen grid size. The method of AP shows the same convergence, but a worse threshold performance. The IQML algorithm performs similarly as the considered ML estimator, and additionally approaches the averaged CRB for high SNR. The analytical ML algorithm in beamspace

and the unitary ESPRIT algorithm perform worse for small SNR and do not reach the CRB, which is due to the reduced aperture of the subarrays.

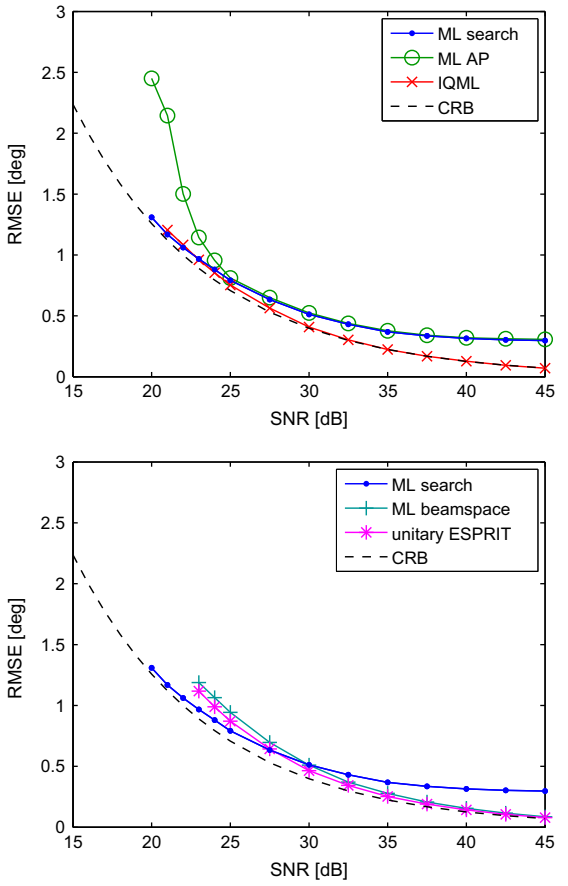

Fig. 4. Performance comparison with two ML implementations (top) and two other algorithms (bottom), averaged RMSE versus SNR, with $\phi_2-\phi_1 = \mathrm{BW}/2$ and $N=1$.

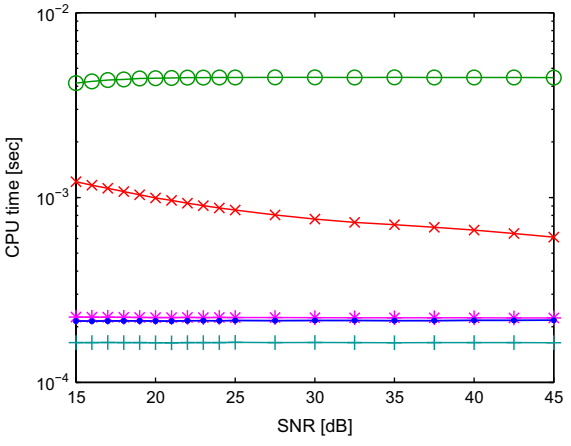

Fig. 5. Computational cost comparison, average CPU time versus SNR, corresponding to the results of Fig. 4.

Regarding computational cost, the simulations have been conducted using MATLAB, version R2010a, on a Windows PC with an Intel Core i7 processor at 2.67 GHz and 4 GB RAM. To the best of our knowledge, the algorithm implementations are fair and efficient. To obtain a general idea of the computational cost, we calculate averaged CPU times using functions tic and toc. To obtain more thorough results, an implementation in C has to be considered. Fig. 5 shows the averaged CPU time versus SNR, corresponding to the results of Fig. 4.

The analytical ML algorithm in beamspace requires the least CPU time, followed by the proposed implementation and unitary ESPRIT. The IQML algorithm performs slower due to its iterative nature. The method of AP is the slowest, as it is both iterative and search-based.

As a result, the developed approach performs comparably to selected computationally efficient algorithms, both in terms of DOA estimation and computational cost. However, it allows a straightforward and non-iterative implementation. In particular, the calculation of the objective function is only based on independent multiply–add operations, which is easily parallelized and therefore well suited for an efficient hardware realization. In contrast, numerically complex operations, such as solving normal equations or an eigendecomposition, can hardly be parallelized.

5. Experimental data analysis

We present results obtained with experimental data from a typical application in automotive radar. The situation with horizontal multipath with a close guardrail, as shown in Fig. 1, is considered. The two propagation paths, according to the observed car and the ghost target, fall into the same processing cell if $r_2-r_1 < \Delta r$, where Δr is the size of a range cell. The range and DOA parameters are related by

$$r_1 \sin(\theta_1) = d_2-d_1$$
$$r_2 \sin(\theta_2) = d_2+d_1$$

where d_1 and d_2 are the normal distances from the guardrail.

The employed short-range radar system operates at a carrier frequency of 24 GHz, and uses a chirp sequence modulation, where each chirp roughly has a duration of 8 μs and a bandwidth of 100 MHz, resulting in a range resolution of 1.8 m [3,8]. For DOA estimation, an array of microstrip patch antennas in the form of a ULA with $M=7$ elements, spaced by $\lambda/2$, is used. A global calibration of channel errors is performed.

A pre-processing procedure to extract relevant processing cells is summarized as follows. An initial DOA is obtained from the peak of the BF spectrum. After detecting cells with significant energy, a clustering procedure of cells with neighboring range, similar relative velocity and initial DOA is used to reduce the number of radar detections. A gating procedure is employed to identify relevant processing cells, i.e., whose relative velocity and initial DOA fall into a desired gate. The described ML estimator for two targets and the GLRT from Section 2.2 are applied to all relevant processing cells. We use a threshold value

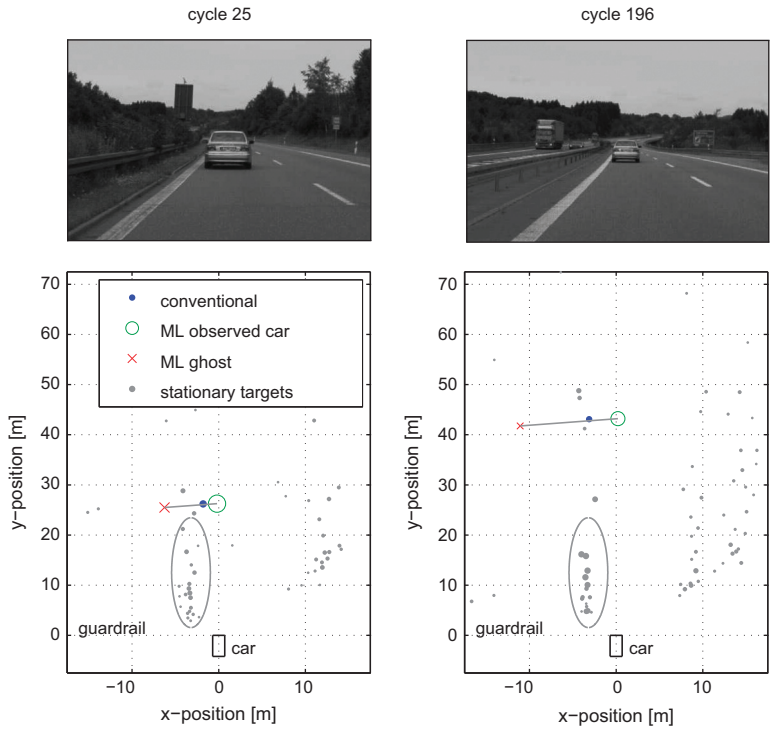

Fig. 6. Experimental data analysis, camera recording of the scene and radar target localization result, for two selected cycles. (For interpretation of the references to color in this figure caption, the reader is referred to the web version of this article.)

$\log \gamma = 1.5M$, which has been obtained from simulations, and according to the Neyman–Pearson principle, this corresponds roughly to a false alarm rate of 0.005 for $\phi_2 - \phi_1 = \mathrm{BW}/2$ and an SNR of 20 dB.

In the selected recording, the car with the radar system is following another car on the left lane of the motorway. In roughly 300 cycles, the distance of the observed car increases from 25 m to 50 m. For two selected cycles, Fig. 6 shows a camera recording of the scene and the result of the radar target localization as a function of x-position and y-position.

Grey dots correspond to stationary targets, while blue dots correspond to moving targets in the relevant gate. For both groups, a single-target DOA has been estimated from the BF spectrum. The result of the proposed ML estimator for two targets is indicated with a green circle and red cross, corresponding to the observed car and ghost target, respectively, as in Fig. 1. On average, the measured power of the ghost target is roughly 6 dB smaller than the power of the observed car. The markersize of all displayed targets is proportional to the measured SNR, which is around 25 dB on average. Note that the indicated stationary target detections can be used to localize the guardrail, which is required to identify the multipath situation.

Fig. 7 shows the DOA estimates of all cycles versus an interpolated range variable, in particular, the conventional results (top), and the improved results (bottom) with ML estimation of two targets and a GLRT.

One can observe that, for the selected scenario, conventional single-target DOA estimation can result in a misleading target localization, in which the target seems to be pulled towards the guardrail. When the multipath propagation is identified correctly, it is possible to apply the proposed ML estimator for two targets and adequately localize the car of interest and a ghost target.

6. Conclusions

We have considered the practically relevant problem of DOA estimation of two targets using a single snapshot. We have proposed a fast implementation of the ML estimator with grid search and interpolation. The fast implementation has been achieved by a simplified calculation of the objective function and pre-calculated projection operators. For saving storage space and computations, we have proposed a rotational shift of the field-of-view such that the relevant angular sector, which has to be evaluated, is delimited and centered with respect to broadside.

The principle has been demonstrated using an example. Simulations have been used to assess the performance of the developed ML estimator, and to compare it among selected representative methods. The performance in terms of DOA estimation and computational cost is roughly comparable to other computationally efficient algorithms, but with an improved threshold performance for closely spaced targets and moderate SNR. Moreover, the developed approach allows a straightforward and non-iterative implementation, which is easily parallelized and therefore well suited for an efficient hardware realization.

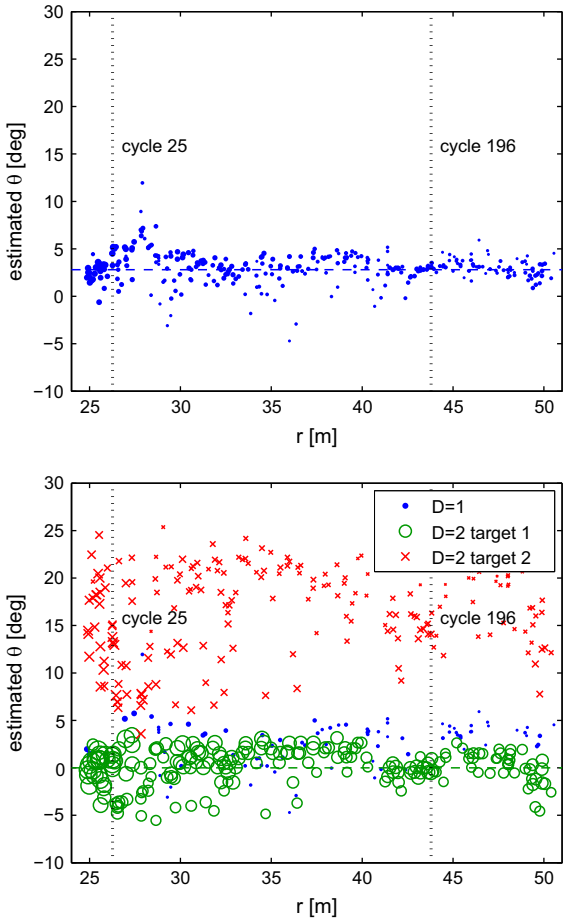

Fig. 7. Experimental data analysis. DOA estimates versus range, conventional results with single-target DOA estimate from BF spectrum (top), improved results with ML estimation of two targets and a GLRT (bottom).

Experimental data has been used to highlight the practical relevance of the developed method.

References

[1] J. Hansen, P. Boyraz, K. Takeda, H. Abut, Digital Signal Processing for In-Vehicle Systems and Safety, Springer, 2011.

[2] F. Gustafsson, Automotive safety systems, IEEE Signal Processing Magazine 26 (4) (2009) 32–47.

[3] H. Winner, S. Hakuli, G. Wolf, Advanced Driver Assistance Systems Handbook (in German: Handbuch Fahrerassistenzsysteme: Grundlagen, Komponenten und Systeme für aktive Sicherheit und Komfort), Vieweg+Teubner, 2009.

[4] V. Winkler, Range Doppler detection for automotive FMCW radars, in: Proceedings of the Fourth European Radar Conference, Munich, Germany, 2007.

[5] F. Gini, A. De Maio, L. Patton, Waveform Design and Diversity for Advanced Radar Systems, IET, 2011.

[6] M. Skolnik, Radar Handbook, McGraw-Hill, 2008.

[7] M. Richards, Fundamentals of Radar Signal Processing, McGraw-Hill, 2005.

[8] M. Wintermantel, Radar system with improved angle formation, Patent Application WO 2010/000252, Germany, 2010.

[9] H. Krim, M. Viberg, Two decades of array signal processing research, IEEE Signal Processing Magazine 13 (4) (1996) 67–94.

[10] D. Barton, Low angle radar tracking, Proceedings of the IEEE 62 (6) (1974) 687–704.

[11] M. Zoltowski, T.-S. Lee, Maximum likelihood based sensor array signal processing in the beamspace domain for low angle radar tracking, IEEE Transactions on Acoustics, Speech and Signal Processing 39 (3) (1991) 656–671.

[12] M. Heuer, A. Al-Humadi, M.-M. Meinecke, R. Mende, Requirements on automotive radar systems for enhanced pedestrian protection, in: Proceedings of the 19th International Radar Symposium (IRS), Warsaw, Poland, 2012.

[13] H. van Trees, Detection, Estimation, and Modulation Theory—Part IV Optimum Array Processing, Wiley and Sons, 2002.

[14] T. Tuncer, B. Friedlander, Classical and Modern Direction-of-Arrival Estimation, Academic Press, 2009.

[15] R. Schmidt, Multiple emitter location and signal parameter estimation, IEEE Transactions on Antennas and Propagation 34 (3) (1986) 276–280.

[16] M. Haardt, J. Nossek, Unitary ESPRIT: how to obtain increased estimation accuracy with a reduced computational burden, IEEE Transactions on Signal Processing 43 (5) (1995) 1232–1242.

[17] G. Golub, C. van Loan, Matrix Computations, The Johns Hopkins University Press, 1996.

[18] S. Pillai, B. Kwon, Forward/backward spatial smoothing techniques for coherent signal identification, IEEE Transactions on Acoustics, Speech and Signal Processing 37 (1) (1989) 8–15.

[19] P. Stoica, A. Nehorai, MUSIC, maximum likelihood, and the Cramér-Rao bound, IEEE Transactions on Acoustics, Speech and Signal Processing 37 (5) (1989) 720–741.

[20] Y. Abramovich, B. Johnson, X. Mestre, Performance breakdown in MUSIC, G-MUSIC and maximum likelihood estimation, in: Proceedings of the 32nd IEEE International Conference on Acoustics, Speech and Signal Processing (ICASSP), Honolulu, USA, 2007.

[21] Y. Bresler, A. Macovski, Exact maximum likelihood parameter estimation of superimposed exponential signals in noise, IEEE Transactions on Acoustics, Speech and Signal Processing 34 (5) (1986) 1081–1089.

[22] J. Li, P. Stoica, Efficient mixed-spectrum estimation with applications to target feature extraction, IEEE Transactions on Signal Processing 44 (2) (1996) 281–295.

[23] I. Ziskind, M. Wax, Maximum likelihood localization of multiple sources by alternating projection, IEEE Transactions on Acoustics, Speech and Signal Processing 36 (10) (1988) 1553–1560.

[24] P. Häcker, B. Yang, Single snapshot DOA estimation, Advances in Radio Science 8 (2010) 251–256.

[25] R. Howell, d-MUSIC: a real time algorithm for estimating the DOA of coherent sources using a single array snapshot, in: Proceedings of the 24th IEEE International Conference on Acoustics, Speech and Signal Processing (ICASSP), Phoenix, USA, 1999.

[26] B. Radich, K. Buckley, Single-snapshot DOA estimation and source number detection, IEEE Signal Processing Letters 4 (4) (1997) 109–111.

[27] A. Thakre, M. Haardt, K. Giridhar, Single snapshot spatial smoothing with improved effective array aperture, IEEE Signal Processing Letters 16 (6) (2009) 505–508.

[28] P. Heidenreich, A. Zoubir, Computational aspects of maximum likelihood DOA estimation of two targets with applications to automotive radar, in: Proceedings of the Fifth Biennial on DSP for In-Vehicle Systems, Kiel, Germany, 2011.

[29] M. Schoor, B. Yang, Local and global calibration for high-resolution DOA estimation in automotive radar, in: Proceedings of the Fifth IEEE Sensor Array and Multichannel Signal Processing Workshop (SAM), Darmstadt, Germany, 2008.

[30] P. Heidenreich, A. Zoubir, High-resolution direction finding of coherent sources in the presence of model errors using alternating projections, in: IEEE Workshop on Statistical Signal Processing (SSP), Cardiff, UK, 2009.

[31] H. van Trees, Detection, Estimation and Modulation Theory—Part I, Wiley and Sons, 1968.

[32] P. Heidenreich, Antenna Array Processing: Autocalibration and Fast High-resolution Methods for Automotive Radar, Ph.D. Thesis, Technische Universität Darmstadt, 2012.

[33] B. Ottersten, M. Viberg, P. Stoica, A. Nehorai, Exact and large sample ML techniques for parameter estimation and detection in array processing, in: Radar Array Processing, Springer-Verlag, 1993.

[34] A. Lee, Centrohermitian and skew-centrohermitian matrices, Linear Algebra and its Applications 29 (1980) 205–210.

[35] M. Pesavento, A. Gershman, M. Haardt, Unitary root-MUSIC with a real-valued eigendecomposition: a theoretical and experimental performance study, IEEE Transactions on Signal Processing 49 (5) (2000) 1306–1314.

[36] P. Heidenreich, A. Zoubir, Computationally simple DOA estimation of two resolved targets with a single snapshot, in: Proceedings of the 37th IEEE International Conference on Acoustics, Speech and Signal Processing (ICASSP), Kyoto, Japan, 2012.